Consecutive Photolyses of Naphthalenedicarboxylic Anhydrides in Low Temperature Matrixes: Experimental and Computational Studies on Naphthynes and Benzocyclopentadienylideneketenes

Tadatake Sato,* Hiroyuki Niino, and Akira Yabe

Photoreaction Control Research Center, National Institute of Advanced Industrial Science and Technology (AIST), AIST Tsukuba Central 5, Higashi 1-1-1, Tsukuba, Ibaraki 305-8565, Japan

Received: February 27, 2001; In Final Form: June 4, 2001

The generation of 1- and 2-naphthynes by the photolyses of 1,2- and 2,3-naphthalenedicarboxylic anhydrides (**1**, **2**), respectively, was investigated by means of Fourier transformed infrared (FT-IR) and ultraviolet−visible (UV−Vis) absorption spectroscopies and theoretical calculations. Consecutive decarboxylation and decarbonylation of **1** were quantitatively analyzed on the basis of UV−Vis absorption spectra. The quantum efficiencies of these processes were estimated as 2×10^{-4} and 0.1, respectively. An isotopomer experiment showed that a cyclopropanone intermediate formed by the decarboxylation showed four C═O stretching bands due to anharmonic resonance. Benzocyclopentadienylideneketene was formed from 1-naphthyne and CO, whereas 2-naphthyne did not react with CO to form the corresponding ketene. This different behavior was discussed on the basis of the geometries and energies calculated at the B3LYP/6-31G** level. Moreover, it was shown that the UV−Vis absorption spectra of reactive intermediates generated in the argon matrix were described well by computations based on INDO/S and time-dependent density functional theory (TD-DFT) methods.

1. Introduction

Arynes, *o*-benzyne and its congeners, have been extensively studied as reactive intermediates for a half century.[1] Among them, *o*-benzyne has been thoroughly characterized by means of matrix isolation spectroscopies.[2] *o*-Benzyne is normally generated by the photolysis or pyrolysis of such precursors as phthalic anhydride and benzocyclobutenedione. In these casees, the simultaneous reaction of *o*-benzyne with carbon monoxide generated in the matrix yields cyclopentadienylideneketene (Scheme 1). This byproduct caused vigorous debate on the assignment of the triple bond stretching vibration in *o*-benzyne. In early work, the IR band at 2085 cm^{-1} had been erroneously ascribed to this vibration,[3] but careful study aided by quantum chemical calculations later showed that this band was actually due to cyclopentadienylideneketene and that the IR band for the triple bond appeared instead at 1846 cm^{-1}.[2] In the studies on *o*-benzyne, stepwise photolysis by means of wavelength-selective irradiation was an effective method for identifying the intermediates produced in the cryogenic matrixes.[4]

Although *o*-benzyne has been studied extensively as described above, matrix isolation and characterization of larger arynes such as naphthyne have seldom been carried out.[5] These didehydrogenated polyaromatic hydrocarbons (PAH) are of interest as reactive intermediates for organic reactions,[6] and as the interstellar compounds responsible for unidentified infrared (UIR) emission bands.[7] Recently, we reported the first direct observation of 1-naphthyne in an argon matrix at 11 K.[8] As in the case of *o*-benzyne, the formation of the corresponding ketene as a byproduct was observed for 1-naphthyne. However, the ketene was not formed from 2-naphthyne. The difference in the behavior of the two naphthynes likely reflects the effect of an additional benzene nucleus fused with *o*-benzyne and is of interest from the viewpoint of the structure−reactivity profile

SCHEME 1

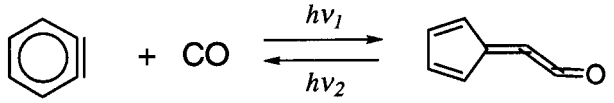

of arynes. In the study on *o*-benzyne and cyclopentadienylideneketene, not only the Fourier transformed infrared (FT-IR) but also the ultraviolet−visible (UV−Vis) spectroscopy of matrix-isolated species contributed significantly to the understanding of the reactions in the matrixes.[4] Although, in the early study, the generation and interconversion of these two compounds were discussed on the basis of comparisons between the actual UV−Vis spectra and the spectra predicted by the semiempirical method with CI expansion,[9] nowadays, more-reliable computational methods are available. Casida et al. have reported that a time-dependent density functional theory (TD-DFT) method can effectively describe the electronic absorption spectra of many molecules with comparatively low computational cost.[10]

Herein, we wish to report the matrix photolyses of 1,2-naphthalenedicarboxylic anhydride (**1**) and 2,3-naphthalenedicarboxylic anhydride (**2**). We used FT-IR and UV−Vis spectroscopies and theoretical calculations to study the reactive intermediates. In particular, the UV−Vis spectra observed in the photolysis of **1** were discussed by comparing the spectra with the theoretical results. We experimented with the several available computational methods (INDO/S, CIS, TD-HF, and TD-DFT) for simulating the electronic absorption spectra and checked the utility of these methods by using the result of consecutive photolysis of **1**. Additionally, the difference in the behavior of the two naphthynes and that of the two ketenes from **1** and **2** was discussed on the basis of the geometries and the energies estimated by means of density functional theory (DFT) calculations.

* Author to whom correspondence should be addressed.

10.1021/jp010746z CCC: $20.00
Published on Web 07/26/2001

SCHEME 2

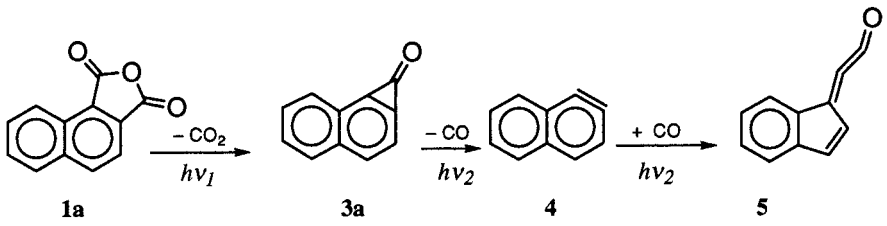

SCHEME 3

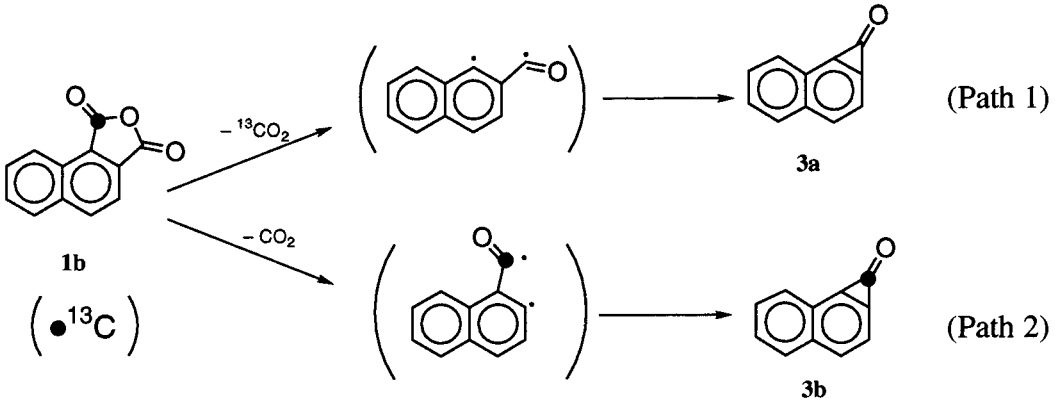

2. Experimental Section

2.1. Materials. 1,2-Naphthalenedicarboxylic anhydride (**1a**) was synthesized from 1,2-dimethylnaphthalene according to the literature procedure.[11] The ^{13}C isotopomer of **1a** (**1b**) was synthesized from 2-methylnaphthalene in the following way. 1-Bromo-2-methylnaphthalene was obtained from bromine and 2-methylnaphthalene by the method of Arnold and Liggett.[12] Then 1-cyano-2-methynaphthalene was obtained from isotopically labeled copper cyanide ($Cu^{13}CN$, Cambridge Isotope Laboratories, 98%) and 1-bromo-2-methylnaphthalene by the method of Friedman and Shechter.[13] 1-Cyano-2-methynaphthalene was oxidized to 1,2-naphthalenedicarboxylic acid and then converted to the anhydride by Dozen's method.[14] The final product was purified by recrystallization from benzene/hexane and sublimation.[15] 2,3-Naphthalenedicarboxylic anhydride (**2**) was purchased from Tokyo Kasei Co. and was purified by recrystallization from acetic acid and sublimation. The purity of these precursors (>97%) was confirmed on the basis of the NMR spectra.

2.2. Matrix Isolation Experiments. Matrix isolation experiments were performed with a closed-cycle helium cryostat (Air Products Displex CS-202). Pressure in the sample chamber was kept at $10^{-6}-10^{-7}$ Torr during the experiments. For FT-IR measurement, a CsI plate cooled to 11 K was used as a substrate, on which vaporized **1** or **2** was co-deposited with argon (99.9999%) at 11 K. KBr plates were used as optical windows for FT-IR measurements, which were carried out on a Perkin-Elmer Spectrum-GXI spectrometer with a resolution of 1 cm^{-1}. For the measurement of UV−Vis absorption spectra, a sapphire and quartz plates were used as the substrate and the optical window, respectively. UV−Vis spectra were measured with a Shimadzu UV-3100 spectrometer.

Wavelength-selective photoirradiation was carried out with the following light sources: (1) third harmonic pulses (THG) of a YAG laser (355 nm: Lotis LS-2125 with YHG-34), where the repetition rate and laser fluence were 10 Hz and ca. 4 mJ cm^{-2} $pulse^{-1}$, respectively; (2) fourth harmonic pulses (FHG) of a YAG laser, where the repetition rate and laser fluence were 10 Hz and ca. 3 mJ cm^{-2} $pulse^{-1}$, respectively; (3) a XeCl excimer laser (308 nm: MPB Technologies Inc. PSX-100), where repetition rate and laser fluence were 10 Hz and ca. 1 mJ cm^{-2} $pulse^{-1}$, respectively; and (4) a high-pressure mercury lamp (Ushio, 500 W) with a 20-cm water filter and a UV-cut glass filter (>350, >330, >310, or >290 nm).

2.3. Computational Methods. All DFT calculations were performed with the Gaussian 98 program package.[16] Geometries of compounds were optimized using the B3LYP method[17] and the 6-31G** basis set. For the calculation of the IR spectra of naphthynes, the 6-31++G** basis set was used instead. The nature of the stationary points was assessed by means of vibrational frequency analysis. With geometries thus obtained, calculations of the electronic spectra were computed by means of semiempirical (INDO/S),[18] ab initio (CIS[19] and TD-HF[20]), and TD-DFT[10] methods (the B3LYP method and the 6-31+G* basis set). All of the calculations, except INDO/S, were done on the IBM RS/6000-SP system at the Tsukuba Advanced Computing Center (TACC) and on the IBM 32 node SP system at NIMC. INDO/S calculations were done with the WinMOPAC program package on a personal computer.

3. Results and Discussion

3.1. Confirmation of the Cyclopropanone Intermediate by Means of an Isotopomer Experiment. We previously reported the generation of 1-naphthyne during photolysis of **1a** on the basis of the observed FT-IR spectra and DFT calculations.[8] It was confirmed that decarboxylation and decarbonylation of the anhydride proceeded stepwise by wavelength-selective irradiation (Scheme 2). However, our assignment of the compound formed by the decarboxylation of **1a** was still tentative. This species showed four C═O stretching bands, although only one C═O band was predicted in the theoretical IR spectrum. To confirm the tentative assignment of this intermediate as **3a**, we examined the photolysis of **1b**, a ^{13}C isotopomer of **1a** (Scheme 3), in an argon matrix. The IR spectrum observed upon photolysis at 355 nm is shown in Figure 1 together with the corresponding spectrum of **1a**. In the spectrum of the photolyzed

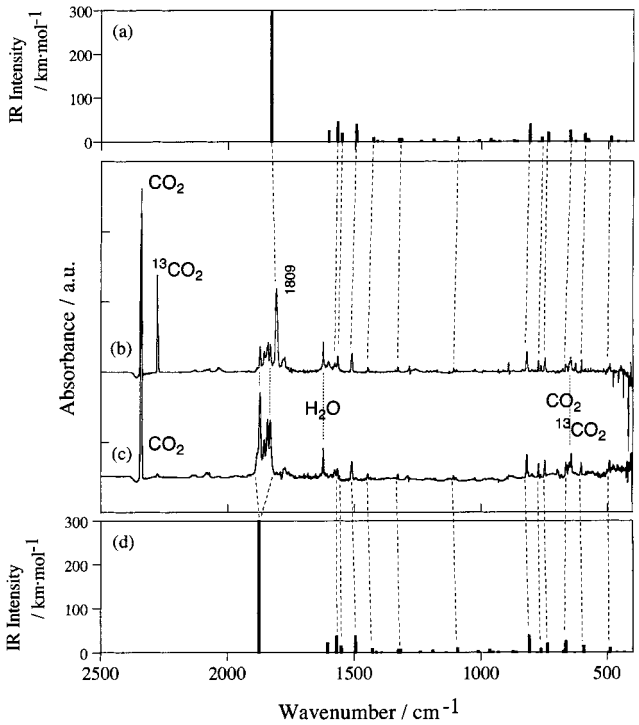

Figure 1. The FT-IR absorption spectra observed upon photolysis of **1b** (b) and **1a** (c) at 355 nm and the theoretical IR spectra (B3LYP/6-31G** level) of **3a** (d) and **3b** (a). The contributions of unchanged **1a** or **1b** were eliminated from the observed spectra.

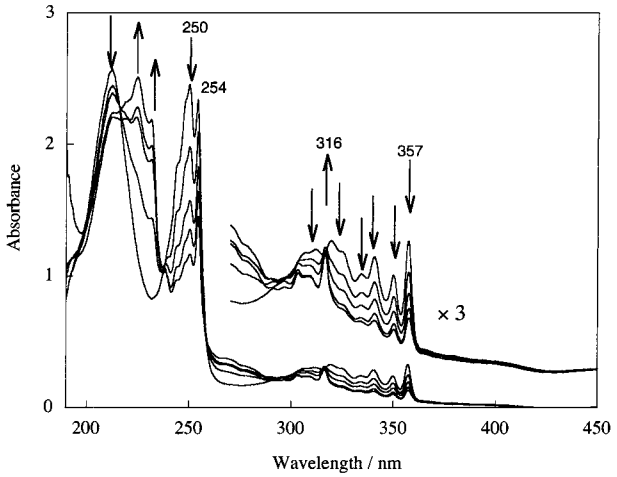

Figure 2. Absorption spectra of **1a** upon irradiation with THG pulses of a Nd:YAG laser (355 nm, 10 Hz, 4 mJ cm^{-2} $pulse^{-1}$) for 0, 1, 3, 6, and 10 h. Arrows show the dynamic behavior in intensity of peaks during irradiation. The band at 254 nm was ascribed to the impurity.

1b, two bands ascribed to CO_2 and $^{13}CO_2$ were observed at 2340 and 2278 cm^{-1}, respectively, and the intensity ratio of $^{13}CO_2/CO_2$ was estimated as 0.42 on the basis of the peak areas. The presence of these two bands revealed the existence of two different decarboxylation pathways, as depicted in Scheme 3: either $^{13}CO_2$ (Path 1) or CO_2 (Path 2) was removed from **1b**. The significant difference was observed in the C═O stretching bands during the reactions of **1a** and **1b**. The intense C═O band observed at 1809 cm^{-1} in photolysis of **1b** was not observed in the photolysis of **1a**. This band was ascribable to the ^{13}C═O stretching mode of the compound formed by Path 2. Moreover, the photolysis of **1b** showed the same four C═O stretching bands observed in the photolysis of **1a**. We ascribed these four bands to the product formed by Path 1 and thus confirmed that the compound formed by the removal of $^{13}CO_2$ from **1b** was identical to that formed by the decarboxylation of **1a**. These results also clearly indicate that **3b** was formed by the removal of CO_2 from **1b**. (The result that there was little change in other IR bands revealed that the skeletal vibrations of the compounds formed by the two paths overlapped one another.) Although the decarboxylation of **1a**, like that of **1b**, should also proceed via two pathways, the decarboxylation resulted in only one product having four C═O stretching bands. This product was identical to the one formed from **1b** by the removal of $^{13}CO_2$. Thus, the splitting of the C═O band in **3a** must be due to anharmonic resonance.[21] The resonance became ineffective because of the isotopic shift of the C═O band to lower wavelength (by 45 cm^{-1} in the calculated IR spectrum). Because there are 18 possible combinations for the resonance in the wavenumber region between 1801 and 1878 cm^{-1} (four IR bands were observed, at 1809, 1833, 1842, and 1873 cm^{-1}), the assignment of combinations was difficult. Thus, the isotopomer experiment confirmed our tentative assignment of the $C_{10}H_6$−C═O species generated by the photolysis of **1a** as **3a**. The spectrum of the product obtained from the photolysis of **3b** was identical to the spectrum of 1-naphthyne generated from **1a**.

3.2. Quantitative Analysis of Consecutive Photolysis of Naphthalenedicarboxylic Anhydrides. We monitored clearly the photolysis of **1a** by means of UV−Vis spectroscopy, and the absorption spectra of **1a** upon irradiation at 355 nm are shown in Figure 2. The lowest transition band of **1a** was observed at 357 nm and was accompanied by vibronic structure. Additionally, the intense peak was observed at 250 nm. As we reported previously, photolysis at 355 nm resulted in decarboxylation of **1a**. Upon irradiation of **1a**, its UV−Vis absorption bands (357, 349, 339, 333, 324, 319, 311, 306, 250, and 211 nm) decreased while new bands ascribed to **3a** increased (316, 309, 303, 296, 290, 278, 268, 231, and 225 nm). The three isosbestic points (around 220, 240, and 295 nm) seen in Figure 2 suggested that the photoinduced conversion of **1a** to **3a** proceeded quantitatively. A sharp peak at 254 nm was due to an unidentified impurity. The result that the absorption band of the impurity did not change during the photolysis indicated that the impurity did not participate in the photoreactions of **1**.[22] It has been reported that the efficiency of photodecomposition of anhydrides decreases as the pressure of a buffer gas increases in the gas phase and that the efficiency approaches zero in a condensed medium.[23] These results reveal that the population of the vibrationally excited state in its ground state, which is the initial state of decarboxylation, decreased because of vibrational relaxation induced by the increased density of the surrounding medium. The efficiency of photoinduced decarboxylation of **1a** could be discussed on the basis of the absorbance change of the absorption band at 357 nm (Figure 3). Since the lowest transition of photoproduct, **3a**, was observed at 316 nm, the change in the absorption band at 357 nm could be observed without spectral overlap with other species. If we assumed that the concentration of **1a** in the matrix was low enough for **1a** to be uniformly photolyzed, i.e., the effect of concentration in the matrix was negligible, we can use the change in absorbance to estimate the quantum efficiency of the process by means of the following equation:[24]

$$A(t) = \log\left[1 + \{10^{(A_0 - A_b)} - 1\} \exp\left(-\frac{2303\epsilon\Phi I_0 t}{h\nu N}\right)\right] + A_b \quad (1)$$

where $A(t)$, A_0, and A_b denote the absorbance at times t and 0,

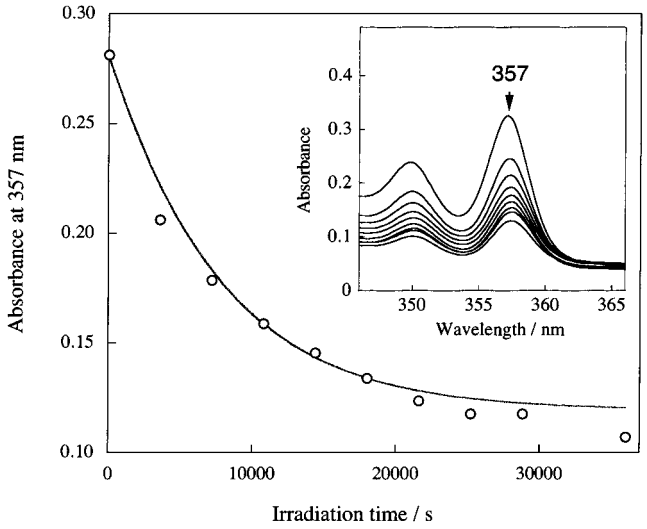

Figure 3. Absorption change at 357 nm (open circle) and fitted result by eq 1 (solid line). Inset: Change in absorption spectra around 357 nm.

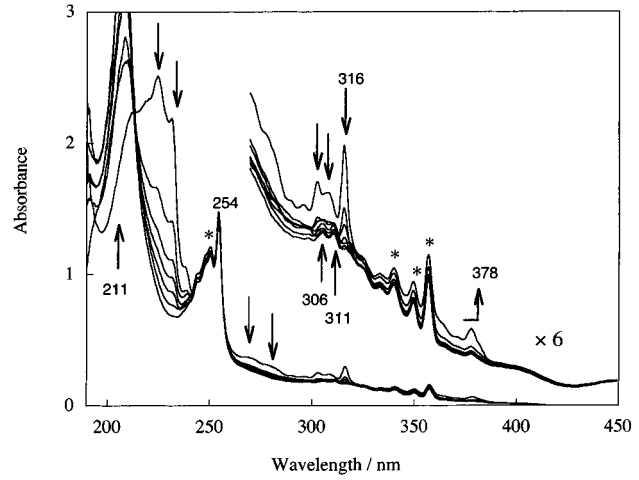

Figure 4. Absorption spectra of **3a** upon irradiation with a high-pressure Hg lamp (>290 nm) for 0, 15, 30, 45, 60, 150 s, and 20 min. Arrows show the dynamic behavior in intensity of peaks during irradiation. The absorption bands marked with asterisks were the contribution of unchanged **1a**. The band at 254 nm was due to the impurity.

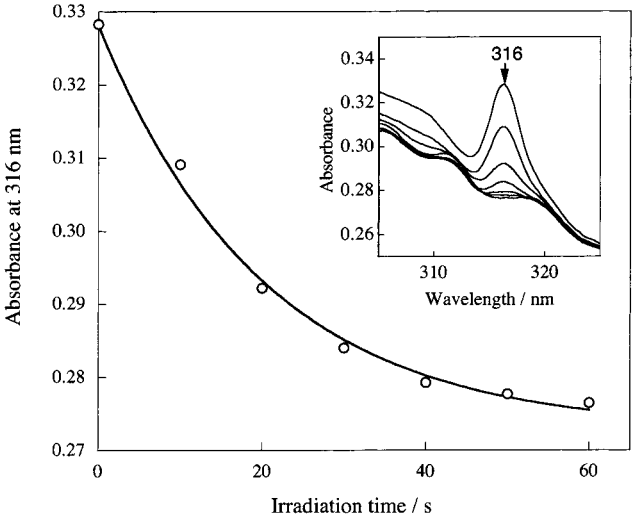

Figure 5. Absorption change at 316 nm (open circle) upon irradiation with a XeCl excimer laser (308 nm, 10 Hz, 1 mJ cm^{-2} $pulse^{-1}$) and fitted result by eq 1 (solid line). Inset: Change in absorption spectra around 316 nm.

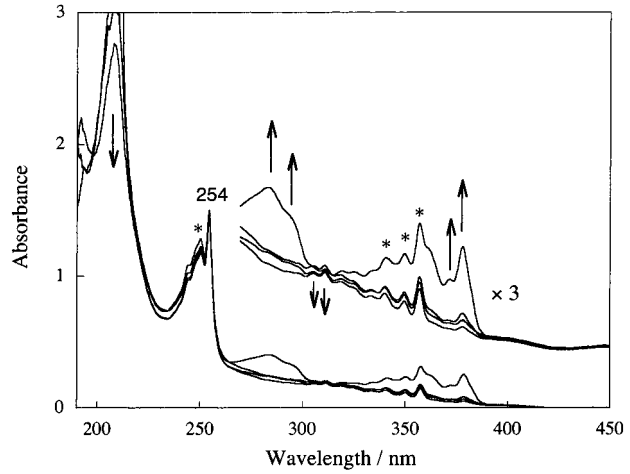

Figure 6. Absorption spectra of **3a** upon irradiation with a high-pressure Hg lamp (>290 nm) for 10 min, 15min, 1 h, and 8 h. Arrows show the dynamic behavior in intensity of peaks during irradiation. The absorption bands marked with asterisks were the contribution of unchanged **1a**. The band at 254 nm was due to the impurity.

and background level, respectively; ϵ [dm^3 mol^{-1} cm^{-1}] is the molar extinction coefficient of the molecule at the monitored wavelength; Φ is the quantum efficiency of the process; I_0 [J cm^{-2} s^{-1}] is the intensity of the irradiated light, where the time-averaged laser power measured by a power meter was used as I_0; and N, h, and ν denote Avogadoro's constant, Planck's constant, and the frequency of the light, respectively. The change in the absorbance at 357 nm shown in Figure 3 was fitted with eq 1. A nonlinear least-squares fitting, where A_b and $\epsilon\Phi$ were chosen as variables, gave the curve shown in Figure 3. The $\epsilon\Phi$ value was estimated as 0.54. When we used the ϵ value estimated for the *n*-hexane solution (2.6×10^3), we estimated the quantum efficiency of the decarboxylation in the matrix as roughly 2×10^{-4}. Photogenerated **3a** was photolyzed with light from a high-pressure mercury lamp (>290 nm) or with a XeCl excimer laser (308 nm), and the resulting changes in the UV−Vis spectra are shown in Figure 4. During this photolysis, the absorption bands ascribable to **3a** disappeared quickly, and a new, strong absorption band at 211 nm appeared. In addition, the increase of very weak absorption bands was observed at 306 and 311 nm. These bands were ascribed to 1-naphthyne (**4**), because the dynamic behavior in their intensities was similar to that of the IR bands ascribed to 1-naphthyne. The band observed at 378 nm was ascribed to benzo[*b*]cyclopentadienylideneketene (**5**), as will be described later. We estimated the quantum efficiency of decarbonylation from the result of the photolysis of **3a** with a XeCl excimer laser. Since the absorption bands of **4** at 306 and 311 nm were very weak, we used the intensity change of the absorption band at 316 nm to estimate the quantum efficiency of decarbonylation. The change in the absorbance at 316 nm with time is shown in Figure 5. In this case, $\epsilon\Phi$ was estimated as 1.8×10^2 from the fitted curve. We estimated the ϵ value at 316 nm as 1.8×10^3 by assuming that all the decarboxylated **1a** was converted to **3a**. Then, the quantum efficiency of the decarbonylation process in the matrix was estimated as roughly 0.1. This relatively high efficiency indicates that this process, unlike the decarboxylation, started from the photoexcited state. The formation of **4** and **5** occurred under similar conditions. Upon prolonged irradiation, the formation of **5**, which we observed in the FT-IR spectrum, was also clearly observed in the UV−Vis spectrum (see Figure 6). The absorption band at 378 nm, which increased slowly upon

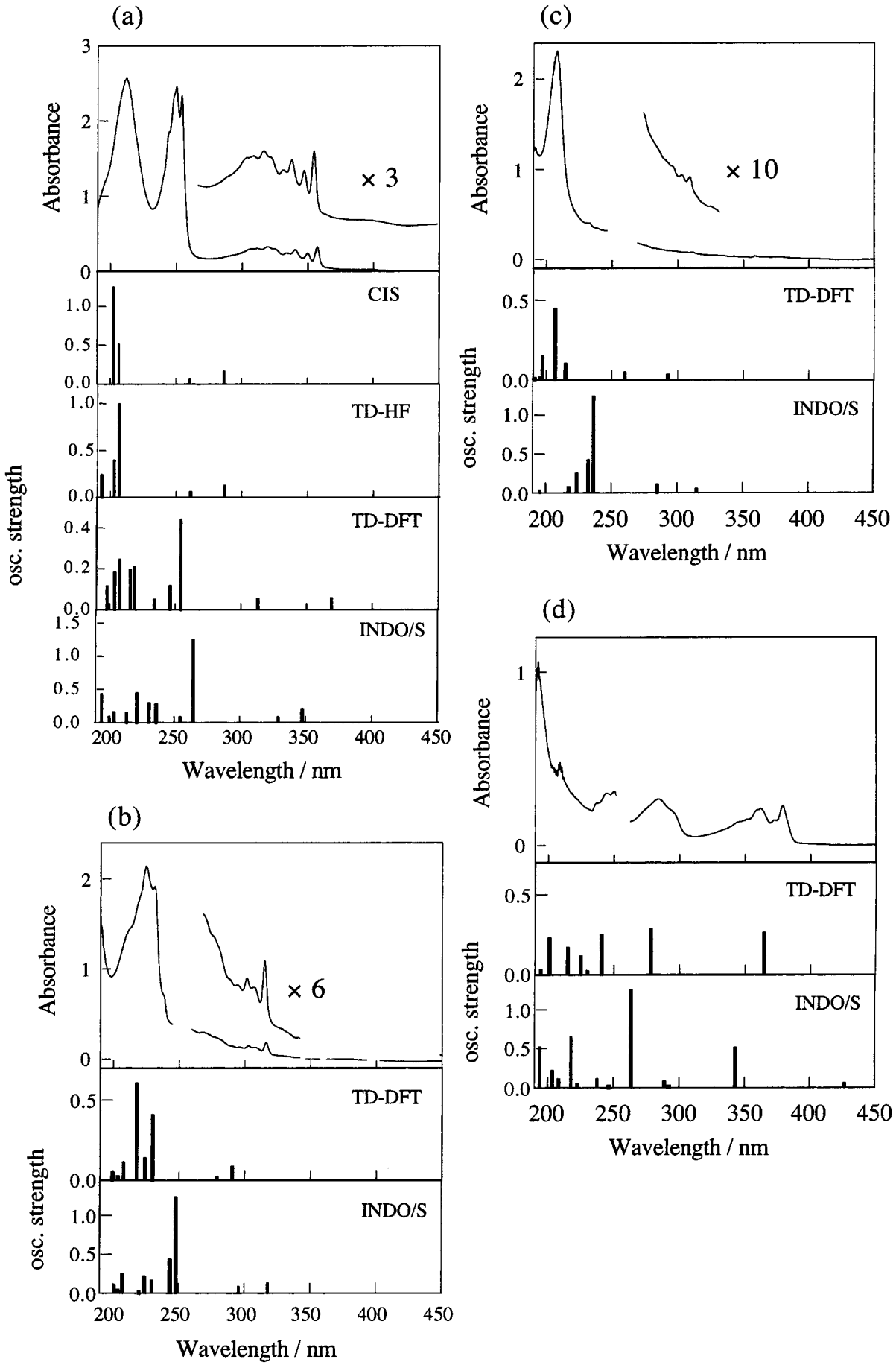

Figure 7. (a) Absorption spectra of **1a** with results calculated by CIS, TD-HF, TD-DFT, and INDO/S methods. Absorption spectra of **3a** (b), **4** (c), and **5** (d) along with results calculated by TD-DFT and INDO/S methods.

SCHEME 4

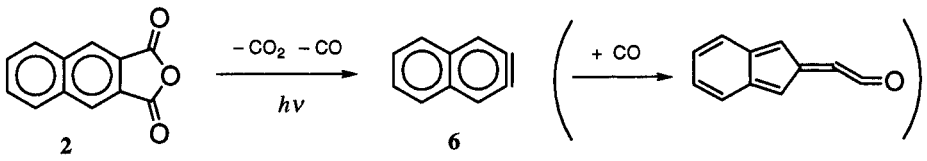

prolonged irradiation, was ascribed to **5**. If **1a** was photolyzed at the shorter wavelength (λ < 310 nm) that caused the decarbonylation of **3a**, the **3a** thus formed would be immediately transformed into **4**. Since the addition of CO to naphthyne occurrs under the same conditions, **4** and **5** are unavoidably formed together. Moreover, the photolysis of the ketene, which was observed for *o*-benzyne,[4] did not occur to 1-naphthyne upon the further shorter wavelength irradiation. Therefore, the wavelength-selective consecutive photolysis was an effective method for observing the spectrum of pure 1-naphthyne.

3.3. Theoretical Investigations of the Electronic Spectra of Reactive Intermediates. We could follow the consecutive photolysis of **1a** clearly by means of UV−Vis spectroscopy, as described above. From the spectra in Figures 2, 4, and 6, the absorption spectra of **1a**, **3a**, **4**, and **5** were extracted and shown in Figure 7. These observed spectra were compared with the spectra predicted by theoretical calculations. For **1a**, the electronic excitation energies and oscillator strengths were calculated by means of CIS, TD-HF, TD-DFT, and INDO/S methods, as shown in Figure 7a. The CIS and TD-HF methods gave almost the same results: these methods overestimate the transition energies. The results obtained by means of TD-DFT and INDO/S methods predicted the lowest transition band at around 350 nm, which was in relatively good agreement with the observed spectrum. The lowest transition energy was described better by the INDO/S method than by the TD-DFT method. However, the absorption bands in the shorter wavelength region (200−250 nm) were reasonably described by TD-DFT method. This tendency was also observed for **3a**, **4**, and **5** (see Figure 7b−d). These results are also in relatively good agreement with the observed spectra. Although theoretical predictions of electronic spectrum result in some discrepancies, calculations by these methods can be a helpful tool for identification of the unusual molecules generated in low-temperature matrixes.

3.4. Photolysis of 2,3-Naphthalenedicarboxylic Anhydride: Formation of 2-Naphthyne. We also examined wavelength-selective irradiation of **2** in an argon matrix. Compound **2** sublimed at 85 °C was co-deposited with argon on the cold substrate at 11 K. The UV−Vis absorption spectra of **2** observed upon irradiation at 266 nm are shown in Figure 8. The lowest transition band of **2** was observed at 348 nm, 8 nm below than that of **1a**. The band at 255 nm would be due to the same impurity as that observed in the photolysis of **1a**. Unlike **1a**, **2** did not undergo selective decarboxylation under any of the reaction conditions. No reaction occurred upon irradiation with THG pulses of a Nd:YAG laser (355 nm). However, direct generation of 2-naphthyne (**6**) was observed (Scheme 4) upon irradiation of **2** with a high-pressure Hg lamp through a UV-cut filter (>310 nm, >330 nm, or >350 nm), with a XeCl excimer laser (308 nm), and with FHG pulses of a Nd:YAG laser (266 nm). Although UV−Vis absorption bands ascribable to **2** decreased upon irradiation at 266 nm, we did not clearly observe the bands ascribable to generated species, except for the band at 224 nm, as seen in Figure 8. However, we did observe the IR bands of the photogenerated species. The difference IR spectrum (Figure 9c) was similar to that previously

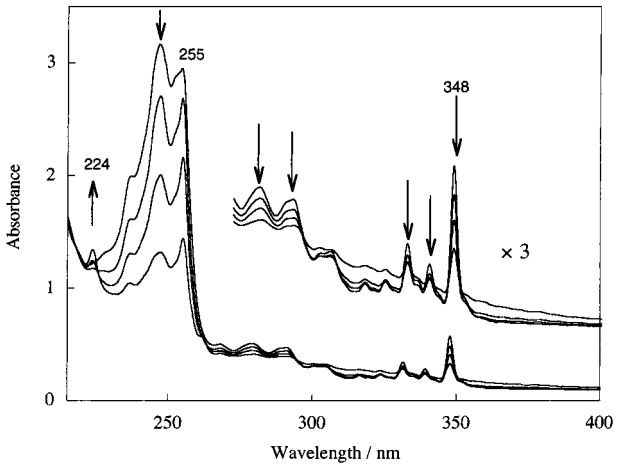

Figure 8. Absorption spectra of **2** upon irradiation with FHG pulses of Nd:YAG laser (266 nm, 10 Hz, 3 mJ cm^{-2} pulse^{-1}) for 0, 30, 90, and 120 min. Arrows show the dynamic behavior in intensity of peaks during irradiation. The band at 254 nm would be due to the impurity.

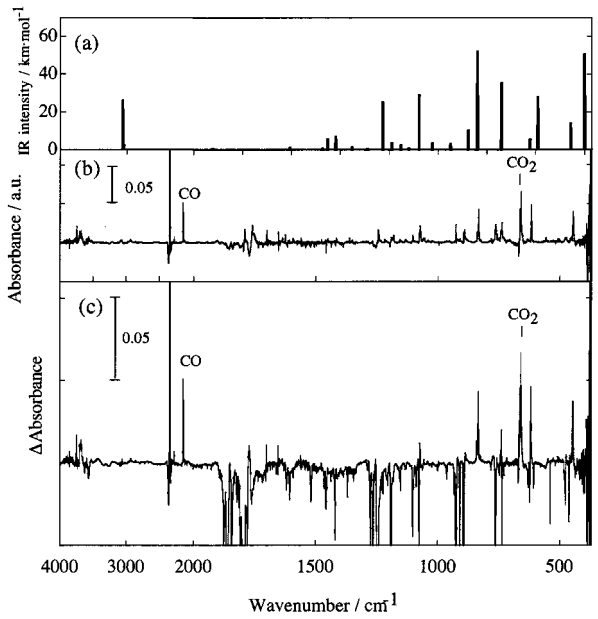

Figure 9. (a) Theoretical IR spectrum of **6** calculated at the B3LYP/6-31++G** level and (b) FT-IR absorption spectra of **6** observed upon irradiation with FHG pulses of Nd:YAG laser: contribution of unchanged **2** was eliminated from the spectrum. (c) Difference IR spectra between those observed before and after irradiation with a high-pressure Hg lamp (>330 nm) for 24 h.

reported.[5c] Figure 9b shows the spectrum obtained by elimination of the contribution of unchanged precursor from the observed one, which corresponds to that of pure photoproduct. This IR spectrum was in good agreement with the theoretical IR spectrum (Figure 9a) predicted by the DFT calculations. Thus, generation of **6** was confirmed. This species was stable under prolonged irradiation at 266 nm. In addition, as shown in Figure 9, the IR band ascribable to ketene was not observed around 2080 cm^{-1} in contrast with **4**.

SCHEME 5

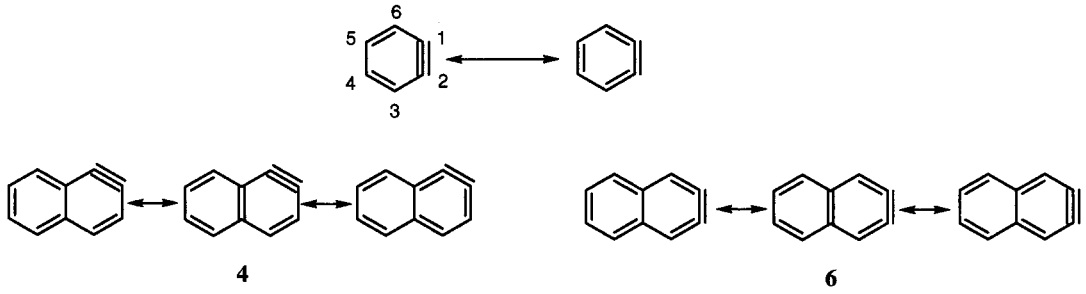

TABLE 1: Calculated (B3LYP/6-31++G level) and Observed Wavenumbers (ν/cm^{-1}) and Relative Intensities (I) for 1- and 2-Naphthynes**

1-naphthyne				2-naphthyne			
ν_{calc}[a]	I_{calc}	ν_{obs}	I_{obs}[b]	ν_{calc}[a]	I_{calc}	ν_{obs}	I_{obs}[b]
403.1	78.5	453.2	m	400.0	50.4	445.9	m
415.3	3.2			455.9	14.1		
500.8	2.6						
550.1	14.8	558.4	m				
569.6	7.7			591.5	27.6	617.5	m
685.9	5.4	696.3	vw	623.1	5.3		
709.6	7.1	717.5	vw				
747.7	32.1	749.3	m	739.7	35.3	737.6	w
773.5	2.5						
797.1	63.1	799.4	m			763.5	w
853.5	4.6			838.2	52.2	833.2	m
861.0	3.1			876.3	10.2	894.4	w
1019.9	6.3			949.0	2.9		
1081.2	19.4	1077.3	vw	1022.5	3.6		
1091.1	8.0	1096.5	vw	1077.2	28.9	1072.8	w
1158.7	2.0			1151.8	2.3	1103.0	vw
1197.5	2.6			1189.2	3.3	1180.7	vw
1216.7	4.8			1226.1	25.1	1244.3	w
1319.8	4.8						
1397.2	3.4			1418.6	6.9	1415.0	vw
1489.6	9.9	1494.7	w	1452.1	5.5	1450.5	vw
1531.4	8.0	1437.2	w				
1609.2	11.6						
3042.6	2.2			3038.6	2.1		
3050.2	9.6						
3062.2	19.7	3028	vw	3054.6	21.5	3060.2	vw
3071.6	12.1	3048.3	vw	3063.3	26.1	3070.0	vw
3080.4	16.9	3088.8	vw	3065.2	7.6	3076.6	vw
				3066.5	12.7	3086.0	vw

[a] The predicted IR bands with intensities > 2 km mol^{-1} are listed. [b] Observed relative intensities. "m", "w", and "vw" represent medium, weak, and very weak, respectively

3.5. Identification of 1- and 2-Naphthynes on the Basis of DFT Calculations. The observed IR bands of the naphthynes are listed in Table 1. The DFT method has been widely used for predicting the IR bands of matrix-isolated species. In particular, the results obtained at the B3LYP/6-31G* level showed good agreement with the experimental results: the overall root-mean-square (rms) deviation for 1066 vibrational modes in 122 molecules has been reported as 34 cm^{-1}.[25] Recently, Kudo et al. reported that the computational results at the B3LYP/6-31++G** level with the scaling using linear function showed extremely good agreement with experimental results (the rms value with this method was 13 cm^{-1}, which was smaller than the best results obtained with constant scaling [21 cm^{-1}]).[26] Kudo et al. argued that the origin of the wavenumber-dependence of the scaling factor was the anharmonicity of the molecular vibrations. We compared our experimental results for naphthynes with the theoretical IR bands calculated at the computational level with Kudo's scaling method (Table 1). According to the previous communication,

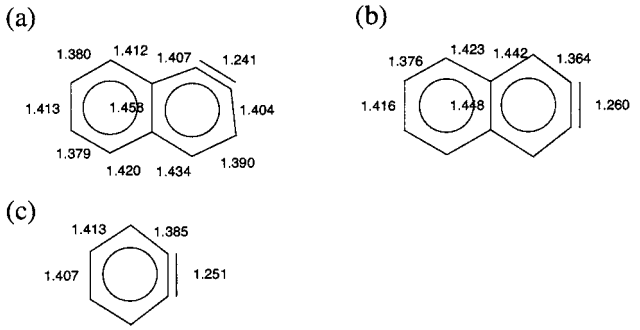

Figure 10. Geometries of (a) **4**, (b) **6**, and (c) *o*-benzyne optimized at the B3LYP/6-31G** level.

the frequency deviations between the observed IR bands and the DFT results (B3LYP/6-31G** level) were within 20 cm^{-1}, except in the case of the band observed at 452 cm^{-1}. This IR band was ascribed to the ring deformation mode containing bending of C−C≡C moiety (See Supporting Information) and the relatively large deviation for this band (which the DFT calculations underestimated by 62 cm^{-1}) may be peculiar to the triple bond in arynes at the computational level. As seen in Table 1, the agreement between calculated and observed IR bands improved when we switched to Kudo's method. The deviation for the band at 452 cm^{-1}, although still large, improved to 50 cm^{-1}. Deviations for other IR bands also improved to within 10 cm^{-1}. In the case of 2-naphthyne, the calculated values also described well the observed wavenumbers.

3.6. Computational Investigations of Naphthynes and Ketenes: Energies and Geometries. The geometries of naphthynes optimized at the B3LYP/6-31G** level are depicted in Figure 10. The triple bond length of *o*-benzyne was estimated as 1.251 Å. This value agrees well with the experimental value of 1.24 ± 0.02 Å estimated by means of a ^{13}C NMR study.[27] Bond lengths of the corresponding triple bonds in 1- and 2-naphthynes were estimated as 1.241 and 1.260 Å, respectively. In addition, the length of the C−C bonds adjacent to the triple bond in the naphthynes differed from those in *o*-benzyne (1.386 Å): these bonds were longer in 1-naphthyne (1.407 and 1.404 Å) and shorter in 2-naphthyne (1.364 Å). Warmuth et al. discussed *o*-benzyne on the basis of the acetylenic and cumulenic mesomers depicted in Scheme 5.[28] They concluded that *o*-benzyne is aromatic with a small amount of bond localization induced by the in-plane π-bond, which results in a structure that is more acetylenic than cumulenic.[28b] Meanwhile, since the resonance in naphthalene can be described by three mesomers, the corresponding mesomers of naphthynes depicted in Scheme 5 show the different character: while two mesomers show acetylenic structure in 1-naphthyne, two cumulenic mesomers are seen in 2-naphthyne. The geometries of the naphthynes reflect the changes in their electronic structures induced by an additional benzene nucleus fused with *o*-benzyne. When conjugation of the additional benzene nucleus occurs in the 3- and

SCHEME 6

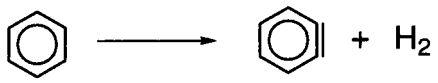

TABLE 2: Energy Difference (kcal/mol) for Dehydrogenetion and Ketene Formation[a]

compounds	dehydrogenation	ketene formation
1-naphthyne	92.03	−36.99
		−36.87
2-naphthyne	94.51	−15.13
o-benzyne	97.21	−27.91

[a] These values were estimated from the energies at the B3LYP/6-31G** level corrected by ZPEs (scaling factor = 0.9804).

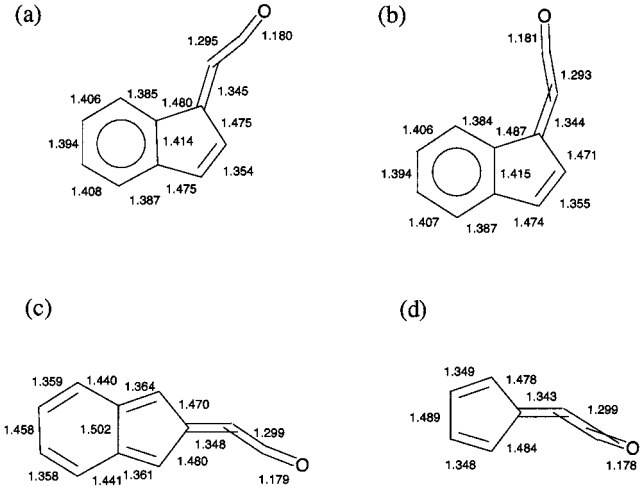

Figure 11. Geometries of (a) **5** (Isomer I), (b) **5** (Isomer II), (c) benzo[*c*]cyclopentadienylidenketene and (d) cyclopentadienylidenketene optimized at the B3LYP/6-31G** level.

4-positions of *o*-benzyne (1-naphthyne), the triple bond is more highly localized compared to that in *o*-benzyne. On the other hand, when conjugation occurs in the 4- and 5-positions of *o*-benzyne (2-naphthyne), the cumulenic character becomes more dominant. The calculated vibrational frequencies of the triple bond stretching mode reflect the difference in the characters, although the calculated intensities are quite weak. The frequencies (and intensities) estimated at the B3LYP/6-31++G** level and scaled with Kudo's method were 1953 (0.36), 1994 (1.33), and 1922 cm^{-1} (0.47 km mol^{-1}) for *o*-benzyne, 1-naphthyne, and 2-naphthyne, respectively. Localization of the triple bond stabilizes the singlet state, and this change was reflected in the singlet−triplet gap in this system.[29] The energy differences for the dehydrogenation (Scheme 6) estimated at the B3LYP/6-31G** level are listed in Table 2. Both naphthynes showed slightly lower energy differences than *o*-benzyne did. These results revealed that even in 2-naphthyne the additional benzene nucleus stabilized the arynes and that 1-naphthyne was more stable than 2-naphthyne because of the localization of the triple bond. The additional benzene nucleus had a larger effect on the ketenes than on the arynes. The geometries of the ketenes optimized at the B3LYP/6-31G** level are shown in Figure 11. As reported for cyclopentadienylideneketene, the bent ketene structures were obtained.[30] The ketene **5** exists as two isomers. However, the difference between the structures is small, and these two isomers show almost identical theoretical IR spectra. In these ketenes, the C−C bond lengths in the additional benzene nucleus are between 1.385 and 1.414 Å, which reveals the delocalization of the π-electrons in this system. On the contrary, bond alternation was clearly

SCHEME 7

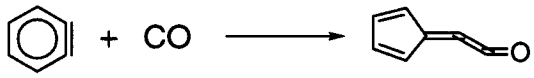

shown in the ketene formed from 2-naphthyne. Accordingly, the stabilization afforded by the delocalization of π-electrons is not effective in this system. The energy differences for the formation of the ketenes from the arynes and carbon monoxide (Scheme 7) are shown in Table 2. The difference for the reaction of 2-naphthyne is much smaller than that for 1-naphthyne. Ketene **5** was stabilized somewhat by the additional benzene nucleus. These results show the thermodymanic stabilities of the compounds. The stabilities are not directly relevant to photochmical reactivities. However, the photochemical reaction in the matrix often gives the same product as that of pyrolysis. Thus, we would be able to get some insights into photochemical reactivity on the basis of the calculated energies. From this viewpoint, the stabilization shown for **5** could explain why the ketene could not be photolyzed to generate 1-naphthyne and carbon monoxide. In contrast, in the ketene formed from 2-naphthyne was destabilized by the additional benzene nucleus. This destabilization could explain why the formation of the ketene was not observed in 2-naphthyne.

4. Conclusion

We followed the photolyses of **1a** and **2** using FT-IR and UV−Vis absorption spectroscopies. Our previous tentative assignment of **3a** was confirmed by means of an isotopomer experiment, which revealed that the C═O band was split into four bands by anharmonic resonance. In addition, we confirmed the generation of 1- and 2-naphthynes by comparing their FT-IR spectra with the improved theoretical IR spectra calculated at the B3LYP/6-31++G** level. By quantitatively analyzing the UV−Vis spectra in the photolysis of **1a**, we showed that the consecutive processes, decarboxylation and decarbonylation, proceeded stepwise with quite different efficiencies, estimated as 2×10^{-4} and 0.1, respectively. Moreover, it is shown that the UV−Vis absorption bands of reactive intermediates in an argon matrix were described well by computations based on the INDO/S and TD-DFT methods. Computational results obtained with these methods should be a helpful tool for the identification of the unusual molecules generated in low-temperature matrixes. The computed geometries of the naphthynes and the ketenes reflect the effect of the additional benzene nucleus fused with *o*-benzyne. In naphthynes, the localization of the triple bond was affected by the position in which the additional benzene nucleus was fused. Moreover, the ketenes showed significant structural differences. We explained the different behavior observed in the two naphthalenedicarboxylic anhydrides on the basis of the effect of the additional benzene nucleus.

Acknowledgment. We are grateful to Dr. Hans P. Reisenauer (Justus-Liebig University of Giessen, Germany) for helpful discussions.

Supporting Information Available: Discussion on the deviation between the calculated and observed IR frequencies in arynes. This information is available free of charge via the Internet at http://pubs.acs.org.

References and Notes

(1) For instance, (a) Hoffmann, R. W. *Dehydrobenzene and Cycloalkynes*; Academic Press: New York, 1967. (b) Levin, R. H. *Reactive*

Intermediates, Vol. 1; Jones, M., Moss, R. A., Eds.; John Wiley & Sons: New York, 1978; Chapter 1.

(2) Radziszewsky, J. G.; Hess, B. A., Jr.; Zahradnik, R. *J. Am. Chem. Soc.* **1992**, *114*, 52, and references therein.

(3) (a) Chapman, O. L.; Chang, C.-C.; Kolc, J.; Rosenquist, N. R.; Tomioka, H. *J. Am. Chem. Soc.* **1975**, *97*, 6586. (b) Dunkin, I. R.; MacDonald, J. G. *J. Chem. Soc., Chem. Commun.* **1979**, 772. (c) Laing, J. W.; Berry, R. S. *J. Am. Chem. Soc.* **1976**, *98*, 660. (d) Nam, H.-H.; Leroi, G. E. *Spectrochem. Acta A* **1985**, *41*, 67. (e) Nam, H;.-H.; Leroi, G. E. *J. Mol. Struct.* **1987**, *157*, 301.

(4) Simon, J. G. G.; Münzel, N.; Schweig, A. *Chem. Phys. Lett.* **1990**, *170*, 187.

(5) (a) Chapman, O. L.; Gano, J.; West, P. R.; Regitz, M.; Maas, G. *J. Am. Chem. Soc.* **1981**, *103*, 7033. (b) Tomioka, H.; Okuno, A.; Sugiyama, T.; Murata, S. *J. Org. Chem.* **1995**, *60*, 2344. (c) Weimer, H. A.; McFarland, B. J.; Li, S.; Weltner, W. Jr. *J. Phys. Chem.* **1995**, *99*, 1824.

(6) (a) Moursounidis, J.; Wege, D. *Aust. J. Chem.* **1988**, *41*, 235. (b) Jung, K.; Koreeda, M. *J. Org. Chem.* **1989**, *54*, 5667. (c) Peña, D.; Pérez, D.; Guitián, E.; Castedo, L. *Org. Lett.* **1999**, *1*, 1555, and references therein.

(7) (a) Pauzat, E.; Talbi, D.; Ellinger, Y. *Astron. Astrophys.* **1995**, *293*, 263. (b) Pauzat, E.; Talbi, D.; Ellinger, Y. *Astron. Astrophys.* **1997**, *319*, 318.

(8) Sato, T.; Moriyama, M.; Niino, H.; Yabe, A. *Chem. Commun.* **1999**, 1089.

(9) Münzel, N.; Schweig, A. *Chem. Phys. Lett.* **1988**, 1*47*, 192.

(10) Casida, M. E.; Jamorski, C.; Casida, K. C.; Salahub, D. R. *J. Chem. Phys.* **1998**, *108*, 4439.

(11) (a) Friedman, L. *Organic Syntheses*; John Wiley & Sons: New York, 1973; Col. Vol. 5, p 810. (b) Matsuura, T.; Ishizaka, M.; Hasuda, Y.; Nishi, S. *Macromolecules* **1992**, *25*, 3540.

(12) Arnold, R. T.; Liggett, R. W. *J. Am. Chem. Soc.* **1942**, *64*, 2875.

(13) Friedman, L.; Shechter, H. *J. Org. Chem.* **1961**, *26*, 2522.

(14) Dozen, Y.; Fujishima, S. *Yukigoseigaku* **1972**, *30*, 964 (in Japanese).

(15) Spectroscopic data of **1b** are as follows: ^{1}H NMR ($CDCl_3$) δ 8.88 (1H, dd, $J = 8.4$, 0.8 Hz), 8.33 (1H, d, $J = 8.2$ Hz), 8.07 (1H, dd, $J = 8.4$, 0.2 Hz), 7.95 (1H, dd, $J = 8.2$, 0.8 Hz), 7.86 (1H, td, $J = 8.3$, 0.8 Hz), 7.81 (1H, td, $J = 8.3$, 0.8 Hz); ^{13}C NMR ($CDCl_3$) δ 163.3, (other weak signals were observed at 148.8, 137.4, 130.6, 130.3, 129.0, 125.0, 119.2, and 117.1 ppm); FTIR($\tilde{\nu}$/cm^{-1}) observed in an argon matrix and predicted frequencies (cm^{-1}) and intensities (km mol^{-1}): 505w (498, 11), 580w (568, 10), − (702, 12) 766m (748, 38), − (757, 10), 839m (820, 32), 892s (879, 102), 933m (912, 56), 1127m (1116, 56), − (1125, 6), 1159w (1142, 24), 1177m (1162, 79), 1283 (1258, 244) 1348w (1337, 7), − (1361, 5), 1462 (1444, 17), − (1509, 7), 1527w (1565, 16), 1749s, 1776s (1782, 516), 1841s (1839, 278), − (3072, 15), − (3085, 17) MS *m*/*z*; Observed 199.030 (M^+) Calculated: 199.035.

(16) Frisch, M. J.; Trucks, G. W.; Schlegel, H. B.; Scuseria, G. E.; Robb, M. A.; Cheeseman, J. R.; Zakrzewski, V. G.; Montgomery, J. A., Jr.; Stratmann, R. E.; Burant, J. C.; Dapprich, S.; Millam, J. M.; Daniels, A. D.; Kudin, K. N.; Strain, M. C.; Farkas, O.; Tomasi, J.; Barone, V.; Cossi, M.; Cammi, R.; Mennucci, B.; Pomelli, C.; Adamo, C.; Clifford, S.; Ochterski, J.; Petersson, G. A.; Ayala, P. Y.; Cui, Q.; Morokuma, K.; Malick, D. K.; Rabuck, A. D.; Raghavachari, K.; Foresman, J. B.; Cioslowski, J.; Ortiz, J. V.; Baboul, A. G.; Stefanov, B. B.; Liu, G.; Liashenko, A.; Piskorz, P.; Komaromi, I.; Gomperts, R.; Martin, R. L.; Fox, D. J.; Keith, T.; Al-Laham, M. A.; Peng, C. Y.; Nanayakkara, A.; Gonzalez, C.; Challacombe, M.; Gill, P. M. W.; Johnson, B.; Chen, W.; Wong, M. W.; Andres, J. L.; Gonzalez, C.; Head-Gordon, M.; Replogle, E. S.; Pople, J. A. *Gaussian 98, Revision A.*; Gaussian, Inc.: Pittsburgh, PA, 1998.

(17) (a) Becke, A. D. *J. Chem. Phys.* **1993**, *98*, 5648. (b) Lee, C.; Yang, W.; Parr, R. G. *Phys. Rev. B* **1988**, *37*, 785.

(18) Ridley, J. E..; Zerner, M. C. *Theor. Chim. Acta* **1973**, *32*, 111.

(19) Foresman, J. B.; Head-Gordon, M.; Pople, J. A.; Frisch, M. J. *J. Phys. Chem.* **1992**, *96*, 135.

(20) Casida, M. E. *Recent advances in density functional methods, Vol. 1*; Chong, D. P., Ed.; World Scientific: Singapore, 1995.

(21) Szczeaniak, K.; Person, W. B.; Leszczynski, J.; Kwiatkowski, J. S. *Pol. J. Chem.* **1998**, *72*, 402.

(22) A sharp peak at 254 nm was due to an unidentified impurity. This impurity showed two absorption bands: a sharp one at 254 nm and a broad and weak one at 210 nm. The concentration of the impurity in the matrix must have been low because these absorption bands were not so intense. Moreover, any FT-IR bands corresponding to the impurity were not detected, probably because of low concentration. The absorption bands of the impurity did not change during the photolysis.

(23) Lohmann, J. *J. Chem. Soc., Faraday Trans.* **1971**, 814.

(24) Equation 1 was derived from the following equation defining the quantum yield; $\Phi = -\mathrm{d}M(t)/P(t)\mathrm{d}t$ where $P(t)$ and $-\mathrm{d}M(t)$ denote the number of absorbed photons and the number of photolyzed molecules, respectively. These are connected with absorbance at time, t, $A(t)$, as follows; $P(t) = (I_0/h\nu N)(1-10^{-A(0)})$, $M(t) = A(t)/1000\epsilon$.

(25) Scott, A. P.; Radom, L. *J. Phys. Chem.* **1996**, *100*, 16502.

(26) Kudo, S.; Masao, T.; Nakata, M. *Chem. Phys. Lett.* **2000**, *322*, 363.

(27) Orendt, A. M.; Facelli, J., C.; Radziszewski, J. G.; Horton, W. J.; Grant, D. M.; Michl, J. *J. Am. Chem. Soc.* **1996**, *118*, 846.

(28) (a) Warmuth, R. *Angew. Chem., Int. Ed. Engl.* **1997**, *36*, 1347. (b) Jiao, H. J.; Schleyer, P. V.; Beno, B. R.; Houk, K. N.; Warmuth, R. *Angew. Chem., Int. Ed. Engl.* **1998**, *36*, 22761.

(29) Squires, R. R.; Cramer, C. J. *J. Phys. Chem. A* **1998**, *102*, 9072.

(30) Scott, A. P.; Radom, L. *Chem. Phys. Lett.* **1992**, *200*, 15.